Strong Inland Propagation of Low-Frequency Long Waves in River Estuaries

Guo, Leicheng; Zhu, C.; Wu, Xuefeng ; Wan, Yuanyang; Jay, David A.; Townend, Ian; Wang, Zhengbing ; He, Qing

DOI
10.1029/2020GL089112

Publication date
2020

Document Version
Final published version

Published in
Geophysical Research Letters

Citation (APA)
Guo, L., Zhu, C., Wu, X., Wan, Y., Jay, D. A., Townend, I., Wang, Z., & He, Q. (2020). Strong Inland Propagation of Low-Frequency Long Waves in River Estuaries. *Geophysical Research Letters*, *47*(19), 1-11. Article e2020GL089112. https://doi.org/10.1029/2020GL089112

Geophysical Research Letters

RESEARCH LETTER
10.1029/2020GL089112

Strong Inland Propagation of Low-Frequency Long Waves in River Estuaries

Leicheng Guo[1], Chunyan Zhu[1,2], Xuefeng Wu[1], Yuanyang Wan[3], David A. Jay[4], Ian Townend[5], Zheng Bing Wang[2,6], and Qing He[1]

[1]State Key Laboratory of Estuarine and Coastal Research, East China Normal University, Shanghai, China, [2]Department of Hydraulic Engineering, Faculty of Civil Engineering and Geosciences, Delft University of Technology, Delft, The Netherlands, [3]Shanghai Estuarine and Coastal Research Center, Shanghai, China, [4]Department of Civil and Environmental Engineering, Portland State University, Portland, OR, USA, [5]School of Ocean and Earth Sciences, University of Southampton, Southampton, UK, [6]Marine and Coastal Systems Department, Deltares, Delft, The Netherlands

Key Points:
- High river flow stimulates local generation of significant low-frequency tides particularly in upstream tidal river part of estuaries
- Varying river flows nonlinearly modulate longitudinal variations of MSf amplitude by enhancing fortnightly asymmetry in subtidal friction
- Strong inland penetration of low-frequency tidal waves and surges beyond the limit of incident waves informs management of compound flood

Supporting Information:
- Supporting Information S1

Correspondence to:
L. Guo,
lcguo@sklec.ecnu.edu.cn

Citation:
Guo, L., Zhu, C., Wu, X., Wan, Y., Jay, D. A., Townend, I., et al. (2020). Strong inland propagation of low-frequency long waves in river estuaries. *Geophysical Research Letters*, *47*, e2020GL089112. https://doi.org/10.1029/2020GL089112

Received 9 JUN 2020
Accepted 22 SEP 2020
Accepted article online 28 SEP 2020

Abstract Tidal waves traveling into estuaries are modified by channel geometry and river flow. The damping effect of river flow on incident astronomical tides is well documented, whereas its impact on low-frequency tides like MSf and Mm is poorly understood. In this contribution, we employ a numerical model to explore low-frequency tidal behavior under varying river flow. MSf and Mm are locally generated by frictional mechanisms inside an estuary, and they are larger in amplitude far upstream in tidal rivers and persist landward of the point of tidal extinction. Increasing river flow nonlinearly modulates the longitudinal variations of MSf and Mm amplitudes. This is dynamically explained by flow-enhanced asymmetry in subtidal friction over the spring-neap (MSf) and perigee-apogee (Mm) cycles, respectively. Estuaries act as frequency filters, where low-frequency waves decay at a smaller rate and propagate more inland than high-frequency waves. Strong inland penetration of low-frequency tides informs compound flood management.

1. Introduction

Tides are an important force driving coastal water motions and the associated transport of sediment and contaminants. Examining tidal wave dynamics and long-wave dynamics is vital for coastal management related to coastal floods, fisheries, habitat, and navigation (Kukulka & Jay, 2003; Moftakhari et al., 2017). It has long been understood that tidal waves traveling into shallow estuaries are altered in amplitude and shape due to bottom friction, channel convergence, and river discharge (Cai et al., 2014; Friedrichs & Aubrey, 1994; Godin, 1985; Lanzoni & Seminara, 1998; Savenije et al., 2008). Nontidal forcing such as river discharge modulates tidal wave propagation and deformation. A river flow slows down the incident waves but speeds up the reflected waves (Godin, 1985, 1991; van Rijn, 2011). River flow also enhances wave deformation by prolonging falling tides and shortening rising tides (Godin, 1999; Jay & Flinchem, 1997; Toffolon & Savenije, 2011). Distorted tidal waves are represented by superimposition of more than one constituent, such as M_2 and its harmonics M_4, M_6, and M_8, where M_2 is the largest lunar constituent and the others are forced overtides. These supratidal oscillations have been extensively examined because of their roles in generating tidal asymmetry and consequent influence on sediment transport and estuarine morphology (Gallo & Vinzon, 2005; Godin, 1999; Guo et al., 2016; LeBlond, 1991; Wang et al., 1999, 2002). M_4 amplitude tends to be larger with significant river discharge than in the tide-only situation, because of enhanced nonlinear river-tide interactions (Guo et al., 2015).

The frictional interaction of tides and river flow has other manifestation as well. The mean water level (MWL) has been widely observed to be higher at spring tides than neap tides in tidal river regions of river estuaries, for example, in the Amazon River (Gallo & Vinzon, 2005), Changjiang River (Guo et al., 2015; Zhang, Cao, et al., 2018), Pearl River (Luo et al., 2020; Zhang, Sun, et al., 2018), Columbia River (Jay et al., 2011, 2014), Mahakam River (Buschman et al., 2009; Sassi & Hoitink, 2013), and St. Lawrence River (Godin, 1999). Guo et al. (2015) and Hoitink and Jay (2016) even used this characteristic as a means to define the boundary between tidal river and tidal estuary sections of a river estuary. This fortnightly variation in MWL is ascribed to the MSf tide constituent (a tidal period of 14.7653 days). While there is a small

astronomically generated MSf, virtually all of the fortnightly energy in a river estuary is locally generated by nonlinear interactions.

A limited number of past studies have examined the low-frequency MSf tide and its impact in causing subtidal water level variations (Aubrey & Speer, 1985; Godin, 1991; Jay et al., 2014; LeBlond, 1979; MacMahan et al., 2014; Parker, 1984; Sassi & Hoitink, 2013), but its dynamic behavior and spatial evolution in response to varying rive discharges have received limited attention. This is probably because the low-frequency tides are not accurately resolved by the harmonic analysis method when significant nonstationary river discharge influence is present (Hoitink & Jay, 2016; Matte et al., 2013). Analyzing MSf is technically challenging because it is modulated by nonstationary flow and coastal processes and usually manifests as a band of energy, not the sharp peak assumed by conventional harmonic analysis (Dronkers, 1964; Jay & Flinchem, 1997; Matte et al., 2013, 2014). Although complementary methods, such as the continuous wavelet transform and newly developed NS_TIDE and S_TIDE functions (Matte et al., 2013; Pan et al., 2018), have been applied, low-frequency tides and their dynamics are still insufficiently understood (Guo et al., 2015, Jay et al., 2014).

The Changjiang Estuary provides a useful example of MSf propagation, in part because river flow does not vary strongly on monthly timescales, facilitating estimation of nonlinear tidal motions. The astronomical tidal wave propagates 700 km inland, and the system is divided into a tidal river (Datong to Jiangyin) and a tidal estuary (from Jiangyin seaward) (Figure 1a). The river discharge detected at the tidal wave limit, Datong, varies seasonally between ~10,000 and ~60,000 m^3/s, and the maximum tidal range is ~5.5 m at Niupijiao (Figure 1; Guo et al., 2015). MWL is significantly higher at spring tide during the wet season (May to September), particularly in the tidal river (supporting information Figure S4).

Harmonic analyses using the T_TIDE software (Pawlowicz et al., 2002) during periods of relatively constant river flow show that the astronomical M_2 and S_2 constituents are slightly amplified near the mouth because of reduced water depth in the landward direction and then progressively damped inside the estuary owing to friction and river discharge (Figures 1b and 1c). A significant M_4 overtide is generated inside the estuary, and its amplitudes display nonlinear variations with river discharge (see Figure S5). Compound tides such as MS_4 and MSf are small in amplitude near the mouth but become significant inside the estuary as well, exhibiting longitudinal variations that are distinct from the astronomical constituents. The MSf amplitude is considerably larger throughout the estuary under a high river flow than during low river periods, and it is also larger than the overtide MS_4 during the high river flow period, at least landward of about km 500 (Figure 1e). Similarly, notable MSf tides are detected in the Amazon Estuary, for example, 0.25 m in amplitude at its tidal limit (Gallo & Vinzon, 2005; see Figure S6), and in the Pearl River Delta (Luo et al., 2020). However, how the low-frequency tides behave under varying river discharges and what controls their spatial and dynamic behaviors remain open questions.

Nonlinearity enters tidal systems through the gradient term in the continuity equation and the advection and friction terms in the momentum equation (Parker, 1984, 1991; Speer & Aubrey, 1985; Wang et al., 1999; see section S1). Friction is one of the most important nonlinear effects, and it reduces tidal amplitude and wave celerity in the landward direction (Godin, 1991; Godin & Gutierrez, 1986; Proudman, 1953). Nonlinearity also leads to internal generation of new harmonics and subsequent wave deformation (Parker, 1984, 1991; Proudman, 1953; Wang et al., 1999). Analytical solutions of tidal wave equations have provided a basic framework for our understanding of tidal dynamics (Friedrichs & Aubrey, 1994; Jay, 1991; Lanzoni & Seminara, 1998; Savenije, 2005). These solutions treat tidal propagation as a sinusoidal wave when omitting friction (Green, 1837) or using an iterative polynomial friction representation (Dronkers, 1964; Godin & Gutierrez, 1986; Jay, 1991). But a numerical approach, as used here, provides a more accurate treatment of nonlinearities (van Rijn, 2011). It allows us to explore the spatial evolution of the low-frequency tides in a long river estuary and the controlling effect of river discharge.

2. Model Setup and Settings

We construct a schematized 1-D estuarine model based on the Delft3D software (Figure S1). The model solves the shallow water equations, and it has been widely validated and used in river, estuary, and coastal environments (Lesser et al., 2004). To ensure complete tidal damping and retrieval of low-frequency tides,

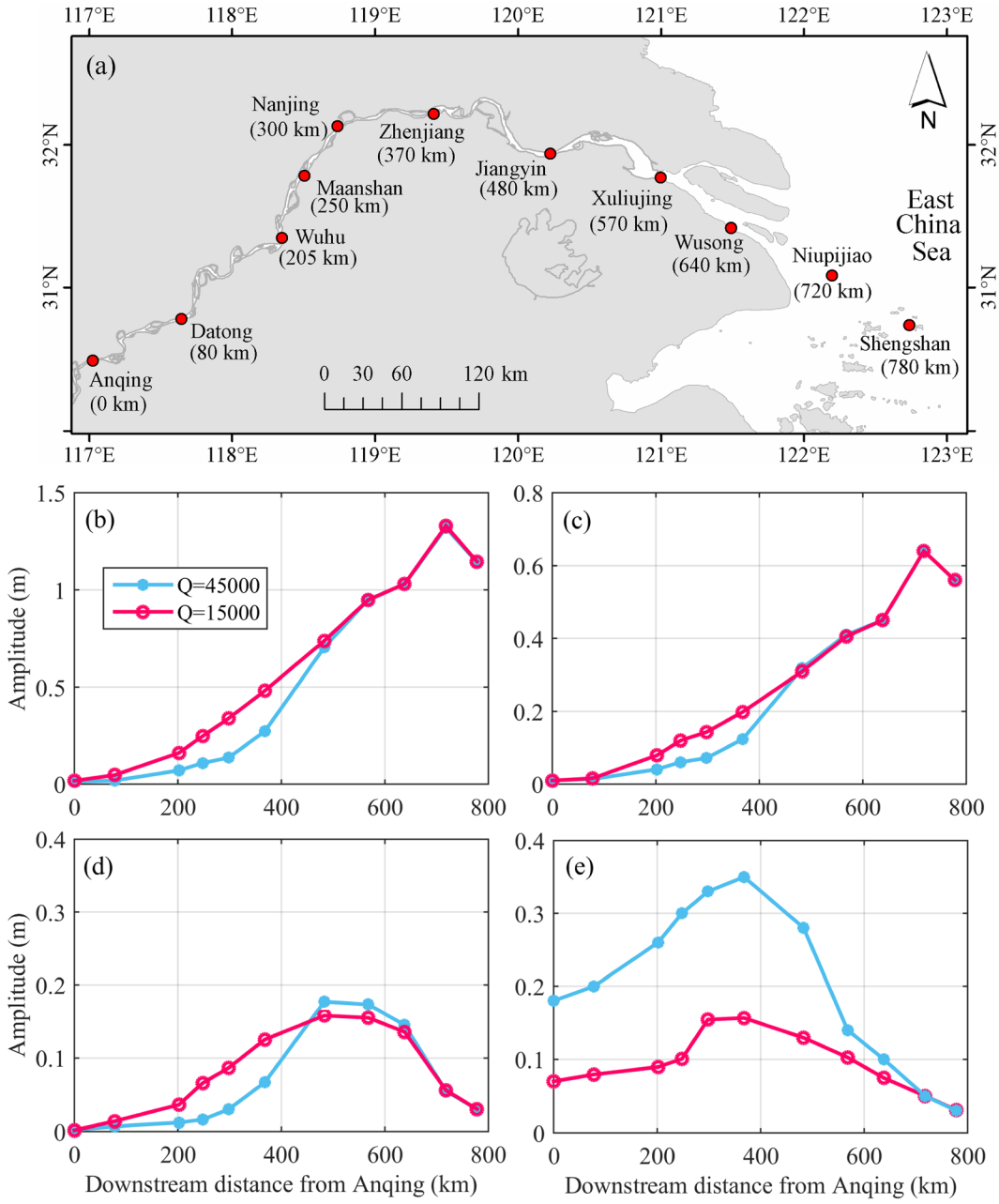

Figure 1. (a) Map of the Changjiang Estuary showing the location of the tidal gauges and along-river variations of the tidal amplitudes of (b) M_2, (c) S_2, (d) MS_4, and (e) MSf in the wet and dry seasons when the mean river discharge is ~45,000 and ~15,000 m^3/s, respectively. A description of the Changjiang Estuary is provided in Guo et al. (2015). The numbers in the brackets in panel (a) indicate that the seaward distance from Anqing River discharge was traditionally monitored at Datong, the tidal wave limit, while water level data at Anqing are included in this work to demonstrate more inland tidal influence.

the model domain is extended to be 1,000 km long with a weakly convergent upstream segment (km 0 to km 600, width varying from 1 to 2 km) and a strongly convergent downstream portion (km 600 to km 1,000, width varying from 2 to 20 km; Figure S1), mimicking the planform of the Changjiang Estuary (Guo et al., 2016; Zhang et al., 2015). Tides and constant river discharges of different magnitudes are prescribed as boundary forcing conditions, which enable stationary tidal output and application of the harmonic analysis approach (Pawlowicz et al., 2002). Note that the 1-D model assumes uniform water

density and excludes tidal flats, which may underestimate tidal asymmetry (Friedrichs & Aubrey, 1994). Tidal asymmetry mainly relates to higher harmonics (overtides), whereas we are interested in the low-frequency tides in this work. Overall, the schematized model provides a virtual lab where tidal dynamic sensitivity to river discharges can be isolated from the influences of basin geometry and irregular shoreline, thus facilitating straightforward exploration of river-tide interactions and low-frequency tidal behavior. Note that varying channel convergence might induce additional tidal amplification or damping (Lanzoni & Seminara, 1998), and regional channel narrowing or width expansion may cause anomalous changes in tidal amplitudes, as that observed in the Changjiang Estuary (see Figure 1b).

A combination of different astronomical harmonics is imposed at the seaward boundary. For simplicity, we input the semidiurnal M_2 and S_2 tides with amplitudes of 1.2 and 0.6 m, respectively. Extra simulations are conducted by including the N_2 tide to reproduce monthly subtidal variations. River discharge is prescribed by constant values of 0, 10,000, 30,000, 60,000, and 90,000 m^3/s, symbolized as Q0, Q1, Q3, Q6, and Q9 scenarios, respectively. A dimensionless parameter, defined by a mean flood tidal discharge to a mean ebb tidal discharge ratio for spring tide at the mouth section, is modeled to be 1.07, 1.03, 0.99, 0.89, and 0.87, respectively, suggesting strong tidal influence even under a high river discharge.

Another improvement here relative to most 1-D tidal models is that we first run a morphodynamic simulation based on the abovementioned model outline when considering M_2 and S_2 tides and a hydrograph with river discharge varying between 10,000 and 60,000 m^3/s, as detailed in Guo et al. (2016). Starting from an initial bed profile, with a linearly varying bed level from 2 to 15 m, morphodynamic equilibrium is approached at the millennial timescale when the bed level change rate become negligible. The eventual equilibrium bed profile is then used as the bottom-level condition in the tidal wave simulations. The purpose of using this equilibrium bed profile (Figure S1) is to provide consistency between the forcing conditions and the morphology as much as possible. Details of the morphodynamic model are referred to Guo et al. (2016).

3. Results

River discharge enlarges the seaward mean current (not shown) and raises the MWL in the upper estuary (Figure 2a). Considerable MWL setup (~0.2 m) and mean currents are still observed in the Q0 scenario, which is ascribed to the Stokes drift generated by a progressive wave (Guo et al., 2016). The landward water level setup and a longitudinal MWL gradient are established to balance the water depth difference and friction asymmetry between flood and ebb tides (Hill, 1994).

River discharge reinforces this intratidal friction asymmetry, and the landward MWL setup becomes more significant (Figure 2a), and a backwater occurs when river discharge is significant. This reduces the tidal volume and compensates it with stored river flow during the flood, which is then evacuated during the ebb (Zhang et al., 2015). In addition, the principal tides are slightly amplified in the lower segment of the estuary owing to channel convergence. The incoming tides are predominantly damped inside the estuary in the landward direction (Figure 2b). A larger river discharge enhances this damping, particularly toward the landward end of the estuary. Accordingly, the tidal wave limit migrates seaward with increasing river discharge, for example, from km 0 in the Q0 scenario to km 300 in the Q9 scenario.

Significant MS_4 and MSf tides are detected inside the estuary (Figures 2c and 2d), as a result of the tidal interactions between M_2 and S_2 tides at their summed and differenced frequencies, respectively. The spatial evolution of the MS_4 tide is similar to the behavior of M_4, as previously reported (Guo et al., 2016). The MSf amplitude increases to ~0.1 m before it reduces slowly more inland in the Q0 scenario (Figure 2d). A river discharge of 10,000 m^3/s results in enlarged MSf throughout the estuary, apart from a small reduction in the utmost landward regions. With further increased river discharges, the MSf amplitude decreases in the upstream regions but keeps increasing in the lower estuary. The location of the maximum MSf amplitude migrates seaward, with an increasingly long upstream tail, below 0.1 m in amplitude, as river discharge increases.

It is notable that the MSf tide remains significant in the upstream regions where both the principal tides and overtides have been dissipated under high river discharges, for example, the region landward of km 300 in the Q3, Q6, and Q9 scenarios. The presence of a significant MSf signal is consistent with and as a result of the fortnightly variations in the MWL (Figure S7).

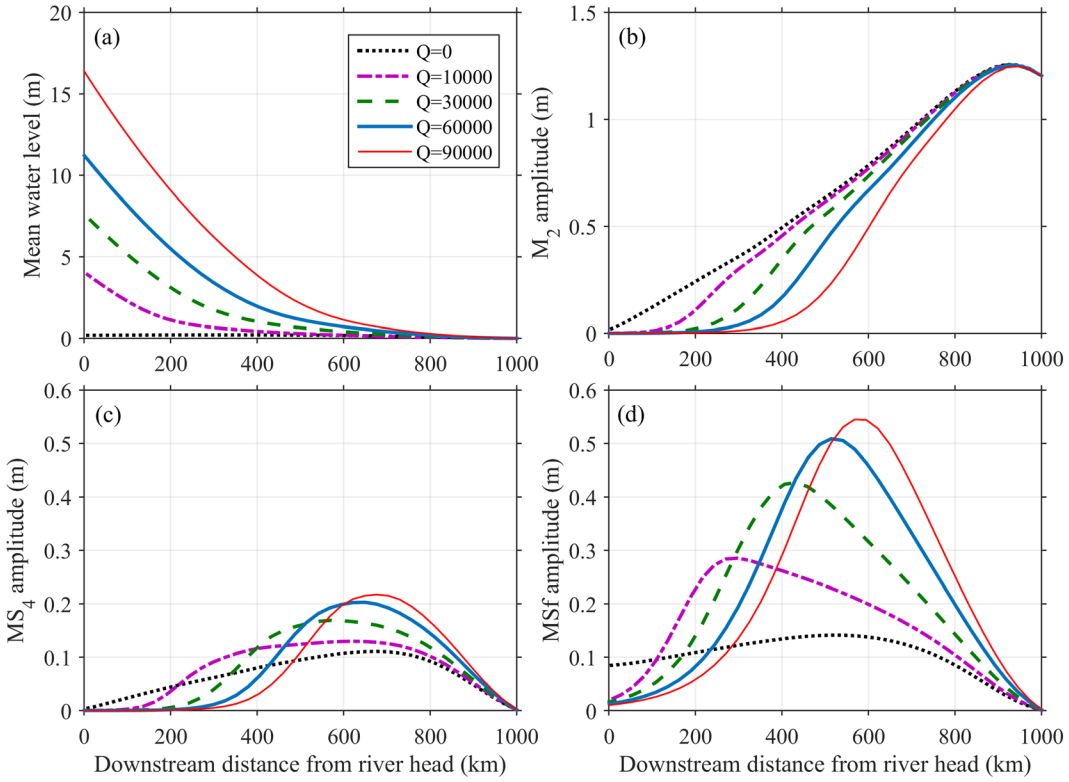

Figure 2. Along-estuary variations of (a) mean water level and amplitudes of (b) M_2, (c) MS_4, and (d) MSf in the scenarios forced by M_2 and S_2 tides under varying river discharges.

Similar results are obtained from the model for MN_4 and Mm constituents (a tidal period of 27.5546 days) in the simulations forced by M_2 and N_2 tides (1.2 and 0.5 m in amplitude, respectively; Figure S8). Significant Mm tide results in an oscillation of the MWL at a monthly timescale (Figure S9), as compared to the fortnightly variations (~14.7 days) related to MSf. This Mm tide is even more difficult to detect accurately from actual data because of its low frequency and variations in river discharge at the comparable monthly timescale. Thus, a modeling approach has strong advantages in isolating tide-induced subtidal water level variations from nontidal signals, especially for Mm.

4. Discussion

Locally detected compound tides are caused by energy transfer from the principal tides to forced constituents. While these forced constituents are insignificant seaward of the estuary, they gain measurable energy and amplitudes inside estuaries. In general, new harmonics with frequencies of $k_1\omega_1 + k_2\omega_2 + k_3\omega_3$ (k_1, k_2, and k_3 can be positive, negative, or null integers; ω_1, ω_2, and ω_3 indicate the frequencies) of the principal constituents can be created through self-, dual-, and triad-tidal interactions (Godin & Gonzalez, 1991; Le Provost, 1991; LeBlond, 1991; Song et al., 2011). The MSf and Mm tides are generated by M_2-S_2 and M_2-N_2 interactions, respectively, at their frequency difference. Thereby, the internally created forced waves enrich and broaden the tidal frequency spectrum in shallow estuarine waters compared to that in open oceans (Guo et al., 2015; Jay et al., 2014), which then requires longer time series of data to resolve them all (Devlin et al., 2014).

Nonlinear friction plays an essential role in the tidal interactions and energy transfer processes (Godin, 1991; Le Provost, 1991; Parker, 1984; Speer & Aubrey, 1985; Wang et al., 1999). The oscillation of the low-frequency signals is affected by friction as well as its long-wavelength nature. Frictional effects increase with decreased depth, increased tidal amplitude, and increased frequency (Parker, 1984). On the one hand, river discharge enhances tidal damping and tidal interaction predominantly through the friction term

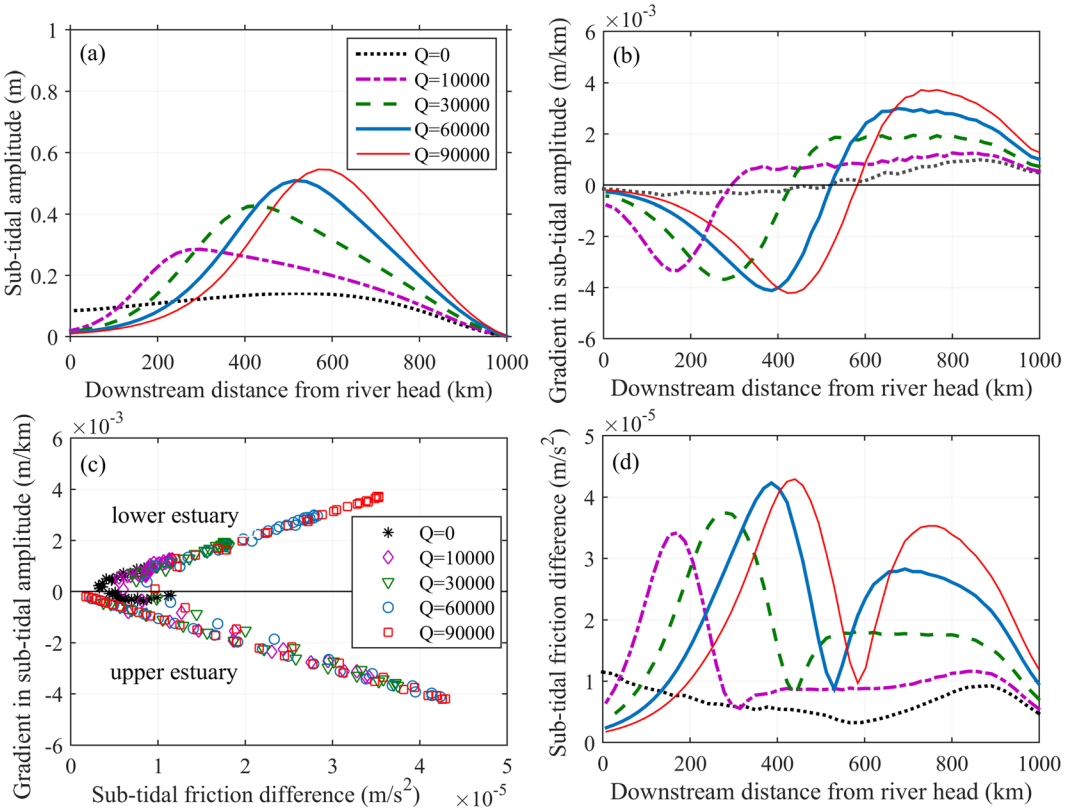

Figure 3. Along-river variations of (a) subtidal water level amplitude, that is, MSf amplitude, (b) longitudinal gradient of the subtidal water level amplitude, (c) the correlation between the subtidal friction difference between spring and neap tides and the spatial gradient of subtidal surface amplitude, and (d) the subtidal friction difference between spring and neap tides.

(Gallo & Vinzon, 2005; Horrevoets et al., 2004; MacMahan et al., 2014). For overtides, larger water depth and smaller friction during high tide lead to larger wave celerity than that during low tide, causing creation of M_4 overtide as regards to M_2 and tidal wave deformation at the daily timescale. For subtidal waves like MSf and Mm, friction is important in their generation because of the shallow water in estuaries but also because, after generation, they are less damped than the higher-frequency constituents. They are generated, because the subtidal friction exhibits variations between spring and neap tides, which call subtidal friction asymmetry (SFA; Figure 3d). The subtidal friction is the low-pass-filtered friction estimated according to inform the friction term in the momentum equation based on the modeled time series of currents and water depth (see section S1). This SFA is the result of nonlinear interactions between tidal currents and water depth, and its fortnightly variations correlate with MSf tide. A similar subtidal friction difference between perigee and apogee cycles is also detected, which correlates with the Mm tide (not shown).

River discharge enhances the SFA because it enlarges the mean currents and increases friction, while also enhanced the difference between flood and ebb tidal currents. Thus the subtidal friction is larger during spring tides than neap tides under significant river discharges, resulting in an asymmetry over the spring-neap cycle (Figure S2). SFA is also larger in the upper estuary where the MSf tide is dissipated in the landward direction than that in the lower estuary. More specifically, SFA is largest at the locations with largest longitudinal gradients in MSf amplitude, both in the upper and lower estuaries (Figures 3b and 3d). SFA is smallest in the middle of the estuary where the MSf amplitude is largest, and its longitudinal gradient is nearly zero. In addition, SFA is larger under higher river discharge than low river discharge. Overall, SFA is highly correlated with the longitudinal gradient in MSf amplitude for all scenarios (Figure 3c). Specifically, a positive gradient in MSf amplitude (indicating a landward amplitude increase) increases concurrently with

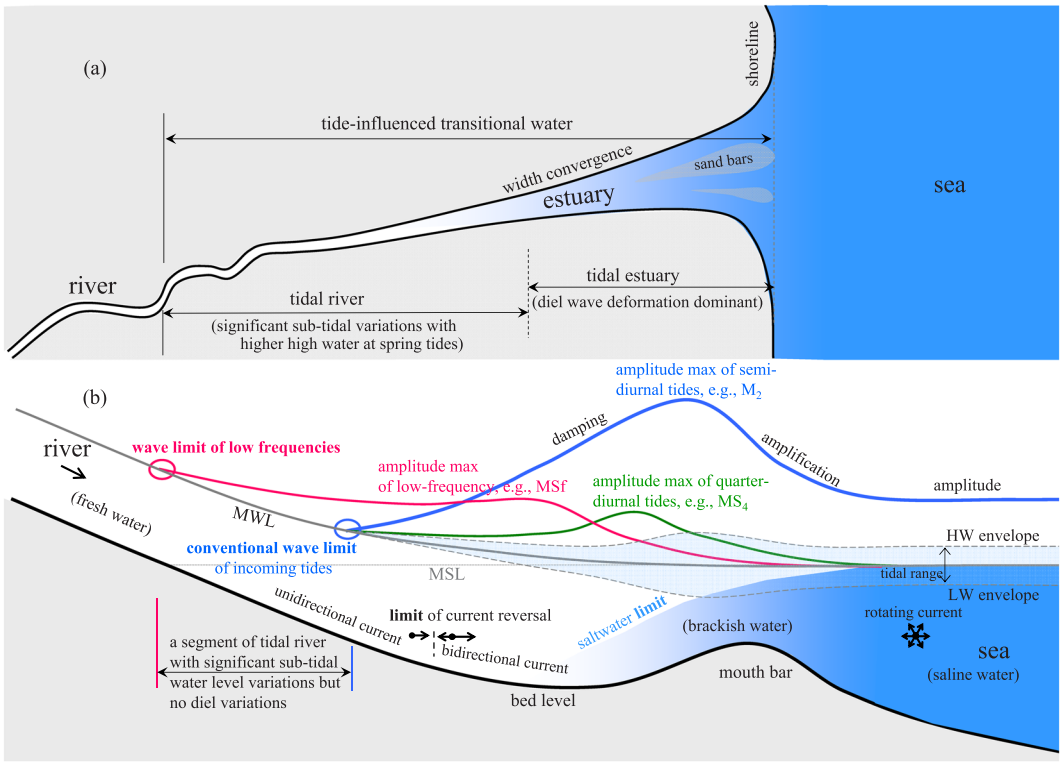

Figure 4. Sketches showing the river-to-ocean transition water in terms of tidal wave properties: (a) the planform and (b) the along-river side view. MSL and MWL indicate mean sea level and mean water level, respectively. HW and LW indicate high water and low water, respectively. The amplitude variations in panel (b) are conceptual and thus are not to the scale.

SFA in the lower estuary seaward of the MSf amplitude maximum. A negative gradient (indicating a landward amplitude decrease) proportionally decreases with SFA in the upper estuary landward of the MSf amplitude maximum. Flow-enhanced subtidal friction and associated spring-neap asymmetry thus explain larger MSf amplitude as river discharge increases (Figure 3a). Dynamically, river-tide interactions enhance the subtidal friction, which needs to be balanced by a subtidal water level gradient in the momentum equation (Buschman et al., 2009; LeBlond, 1978; Sassi & Hoitink, 2013). Therefore, more water is stored in the upper estuary during spring tide (or proxigean tide when talking about Mm) than neap tide, leading to a fortnightly signal in the tidal spectrum.

MSf and Mm are more prominent in the upper estuary, compared to pronounced influence of overtides in the lower estuary. This is because low-frequency waves have a larger length scale and, therefore, decay slowly in the landward direction after their forcing by the main tidal constituent decreases (Figure 4). Henrie and Valle-Levinson (2014) estimated that the subtidal wave length is ~10 times of the estuary length in a ~175 km long subtropical estuary. Thus, the MSf length scale is estimated to be much longer than the physical length of any estuary on earth, based on its period and estuary depth. The long-distance propagation of low-frequency waves can be explained in terms of a 1-D continuity equation:

$$\frac{\partial Q_{MSf}}{\partial x}+\frac{\partial S_{MSf}}{\partial x}=-b\frac{\partial \zeta_{MSf}}{\partial t}\approx 0$$

where b is channel width; Q_{MSf}, ζ_{MSf}, and S_{MSf} are, respectively, the transport, surface elevation, and Stokes drift of the MSf wave. The low-frequency and long-wavelength nature of MSf requires that the divergence of Q_{MSf} and S_{MSf} must balance. Generation of S_{MSf} continues to the head of the tide, and some distance further landward is required for extinction of the MSf oscillation. Moreover, tidal wave propagation is frequency dependent; that is, high frequencies decay at a higher rate than low frequencies

(Godin, 1985). Thus, the MSf tide dissipates at a smaller rate than the M_2 and M_4 constituents inside estuaries, confirming the role of an estuary as a frequency filter (Godin, 1985; Kennedy, 1984). As a result, the low frequencies can travel hundreds of kilometers further inland than the principal tides (Figures 2 and 4). Finally, the above equation suggests that MSf and Mm (and similar motions) are actually oscillations rather than waves, because the divergence of the transport Q_{MSf} is balanced by the divergence of S_{MSf}, not changes in surface elevation ζ_{MSf}.

It remains an open question how further inland the low-frequency tides can penetrate until they are dissipated under the combined influence of river discharge, bed level, and tidal strength (Kästner et al., 2019; Tanaka et al., 2014). River stage increases with increasing river discharge; thus, the along-river MWL gradient becomes larger under a higher river discharge condition. This larger MWL gradient constrains landward tidal wave propagation and enhances tidal damping (Cai et al., 2016). It is notable that alluvial estuaries with significant river discharges usually have a long tide-influenced reach because of the low-lying landscape in the river-to-ocean transition zone (Gugliotta & Saito, 2019), such as the Amazon Estuary (~1,100 km long; Gallo & Vinzon, 2005) and the Changjiang Estuary (~700 km long, Guo et al., 2015). In such cases, the river bed elevation at the limit of incoming astronomical tides may be still below the mean sea level in the coastal ocean, facilitating inland wave propagation (Kästner et al., 2019). The low-lying lower river also provides space for incoming tidal waves to adjust their amplitude and shape to accommodate the variations of river discharges and friction at different timescales (Zhang et al., 2015). Moreover, a backwater water surface profile is more likely to occur in such cases than drawdown of the surface profile (Lamb et al., 2012). Overall, low-frequency waves are then more pronounced in low-lying coastal plain river estuaries, when compared to tide-dominated estuaries with relatively shorter physical length and small river discharge. It is likely that the extinction point for subtidal oscillations in long alluvial estuaries conforms to the analysis of Kästner et al. (2019) for astronomical tides—the propagation of the low-frequency waves is extinguished when river bed reaches a height of the mean sea level. However, the inland propagation and extinction of low-frequency waves in estuaries of varying length and bed level profiles would merit future study.

Inland propagation of low-frequency waves indicates that marine and tidal influences can reach upstream rivers well beyond the landward limit of astronomical tides, which is already far beyond the limit of salt intrusion and limit of current reversal in large river estuaries (Figure 4). Moreover, the backwater effect that the ocean exerts on the river outflow extends even further upstream. For example, the backwater effect has been estimated to extend ~800 km in the lower Mississippi River where the tides are small (Lamb et al., 2012). The backwater effect is also substantial in the Changjiang Estuary though the landward limit of its influence has not been quantified (Zhang et al., 2016). More inland influences of low-frequency waves and backwater effect suggest the need to revisit the definition and spatial extent of a tidal river than conventionally assumed based on salt intrusion limit (Pritchard, 1967) and wave limit of astronomical tides (Fairbridge, 1980) (Figure 4).

Understanding the low-frequency tides has implications for tidal prediction, calculation of extreme high water level inundation risk, subtidal mixing and water exchange, and management of tidal river ecosystem (Guo et al., 2016; Jay et al., 2014; MacMahan et al., 2014; Prandle, 1991). For example, the MWL and the extreme high water level become much higher at proxigean spring tide compared with the situation without low-frequency tides, for example, up to 0.5 m higher in the upper Changjiang Estuary. Similarly, low-frequency surges and tsunami waves also can propagate more inland in river estuaries (Tolkova, 2017). Thus, long inland propagation of the low-frequency long waves needs to be considered in assessment of extreme high water level and management of compound floods in river estuaries with significant river-tide interaction. Also, the presence of significant subtidal MWL variation can affect river discharge estimation based on river stage-discharge rating curves. River stage monitoring is technically easier than cross-sectional velocity measurement, but tide-induced subtidal MWL variations can induce associated spurious river discharge variations. Therefore, river discharge data obtained at the tidal wave limit of principle tides may need to be filtered to remove the subtidal influences.

5. Conclusions

Daily averaged MWL is often higher at spring tides than neap tides in the upper regions of estuaries influenced by significant river discharges, such as the Changjiang, Columbia, and Amazon estuaries. In this

work we employed a numerical model to investigate this phenomenon and the low-frequency tidal behavior. We found that significant low-frequency tides such as MSf and Mm are locally generated (within the estuary), especially when river flow is high. Increased river discharge enhances the low-frequency tides because the river-tide interaction reinforces the subtidal fiction and the difference between friction at spring and neap tides. The amplitude maxima of the MSf tide are located further upstream than that of the principal (astronomical) tides and their overtides. Its spatial behavior is explained by a subtidal friction difference between spring and neap tides (for MSf) and between perigee and apogee cycles (for Mm). Subtidal variation in MWL persists in the river upstream of the tidal wave limit of the principal tides, which suggests more inland tidal influence than conventionally assumed, and implies a need to revisit the definition and spatial extent of a tidal estuary or tidal river. Though simple and highly schematized, our model results reveal ubiquitous low-frequency tidal behavior in response to different river discharges, and the findings inform prediction and interpretation of extreme high water levels during compound flooding in estuaries.

Data Availability Statement

No new data are used in this work, and the tidal height data are collected from official websites of state water resources department (http://221.226.28.67:88/jsswxxSSI/Web/Default.html?m=2) (in Chinese), are available through Guo et al. (2015), and are archived in PANGAEA (https://issues.pangaea.de/browse/PDI-25360).

Acknowledgments

This work is supported by the project "Coping with deltas in transition" within the Programme of Strategic Scientific Alliances between China and the Netherlands (PSA), financed by the Ministry of Science and Technology of the People's Republic of China (MOST) (No. 2016YFE0133700) and the Royal Netherlands Academy of Arts and Sciences (Koninklijke Nederlandse Akademie van Wetenschappen [KNAW]) (No. PSA-SA-E-02), and also partly by MOST (No. 2017YFE0107400), the National Natural Science Foundation of China (Nos. 51739005 and 41876091), Science and Technology Commission of Shanghai Municipality (Nos. 18DZ1206400, 19QA1402900, and 20DZ1204700), and the Fundamental Research Funds for the Central Universities. We thank two anonymous reviewers for their constructive comments and suggestions.

References

Aubrey, D. G., & Speer, P. E. (1985). A study of non-linear tidal propagation in shallow inlet/estuarine systems. Part I: Observations. *Estuarine, Coastal and Shelf Science*, *21*, 185–205. https://doi.org/10.1016/0272-7714(85)90096-4

Buschman, F. A., Hoitink, A. J. F., van der Vegt, M., & Hoekstra, P. (2009). Subtidal water level variation controlled by river flow and tides. *Water Resources Research*, *45*, W10420. https://doi.org/10.1029/2009WR008167

Cai, H. Y., Savenije, H. H. G., Jiang, C. J., Zhao, L. L., & Yang, Q. S. (2016). Analytical approach for determining the mean water level profile in an estuary with substantial freshwater discharge. *Hydrology Earth System Science*, *20*, 1177–1195. https://doi.org/10.5194/hess-20-1177-2016

Cai, H. Y., Savenije, H. H. G., & Toffolon, M. (2014). Linking the river to the estuary: Influence of river discharge on tidal damping. *Hydrology and Earth System Science*, *18*, 287–304. https://doi.org/10.5194/hess-18-287-2014

Dronkers, J. J. (1964). *Tidal computations in rivers and coastal waters* (pp. 219–304). North-Holland, Amsterdam: Interscience (Wiley).

Fairbridge, R. W. (1980). The estuary: Its definition and geochemical role. In E. Olausson & I. Cago (Eds.), (pp. 1–35). John Wiley, New York: Chemistry and geochemistry of estuaries.

Friedrichs, C. T., & Aubrey, D. G. (1994). Tidal propagation in strongly convergent channels. *Journal of Geophysical Research*, *99*, 3321–3336. https://doi.org/10.1029/93JC03219

Gallo, M. N., & Vinzon, S. B. (2005). Generation of overtides and compound tides in the Amazon estuary. *Ocean Dynamics*, *55*(5–6), 441–448. https://doi.org/10.1007/s10236-005-0003-8

Godin, G. (1985). Modification of river tides by the discharge. *Journal of Waterway, Port, Coastal and Ocean Engineering*, *111*(2), 257–274. https://doi.org/10.1061/(ASCE)0733-950X(1985)111:2(257)

Godin, G. (1991). Frictional effects in river tides. In B. B. Parker (Ed.), *Tidal hydrodynamics* (pp. 379–402). Toronto: John Wiley.

Godin, G. (1999). The propagation of tides up rivers with special consideration of the upper Saint Lawrence River. *Estuarine, Coastal and Shelf Science*, *48*(3), 307–324. https://doi.org/10.1006/ecss.1998.0422

Godin, G., & Gonzalez, I. (1991). About some very small harmonics which are present in the tide of the Pacific. *Deutsche Hydrografische Zeitschrift*, *44*(3), 115–132.

Godin, G., & Gutierrez, G. (1986). Nonlinear effects in the tide of Bay of Fundy. *Continental Shelf Research*, *5*(3), 379–402. https://doi.org/10.1016/0278-4343(86)90004-X

Green, G. (1837). On the motion of waves in a variable canal of small depth and width. *Transactions of the Cambridge Philosophical Society*, *6*, 457–462.

Gugliotta, M., & Saito, Y. (2019). Matching trends in channel width, sinuosity, and depth along the fluvial to marine transition zone of tide-dominated river deltas: The need for revision of depositional and hydraulic models. *Earth-Science Reviews*, *191*, 93–113. https://doi.org/10.1016/j.earscirev.2019.02.002

Guo, L. C., van der Wegen, M., Jay, D. A., Matte, P., Wang, Z. B., Roelvink, J. A., & He, Q. (2015). River-tide dynamics: Exploration of nonstationary and nonlinear tidal behavior in the Yangtze River estuary. *Journal of Geophysical Research: Oceans*, *120*, 3499–3521. https://doi.org/10.1002/2014JC010491

Guo, L. C., van der Wegen, M., Wang, Z. B., Roelvink, J. A., & He, Q. (2016). Exploring the impacts of multiple tidal constituents and varying river flow on long-term, large scale estuarine morphodynamics by means of a 1D model. *Journal of Geophysical Research: Earth Surface*, *121*, 1000–1022. https://doi.org/10.1002/2016JF003821

Henrie, K., & Valle-Levinson, A. (2014). Subtidal variability in water levels inside a subtropical estuary. *Journal of Geophysical Research: Oceans*, *119*, 7483–7492. https://doi.org/10.1002/2014JC009829

Hill, A. E. (1994). Fortnightly tides in a lagoon with variable choking. *Estuarine, Coastal and Shelf Science*, *38*, 423–434. https://doi.org/10.1006/ecss.1994.1029

Hoitink, A. J. F., & Jay, D. A. (2016). Tidal river dynamics: Implications for deltas. *Reviews of Geophysics*, *54*, 240–272. https://doi.org/10.1002/2015RG000507

Horrevoets, A. C., Savenije, H. H. G., Schuurman, J. N., & Graas, S. (2004). The influence of river discharge on tidal damping in alluvial estuaries. *Journal of Hydrology*, *294*, 213–228. https://doi.org/10.1016/j.jhydrol.2004.02.012

Jay, D. A. (1991). Green's law revisited: Tidal long-wave propagation in channels with strong topography. *Journal of Geophysical Research*, *96*, 20,585–20,598.
Jay, D. A., & Flinchem, E. P. (1997). Interaction of fluctuating river flow with a barotropic tide: A demonstration of wavelet tidal analysis methods. *Journal of Geophysical Research*, *102*(C3), 5705–5720. https://doi.org/10.1029/96JC00496
Jay, D. A., Leffler, K., & Degens, S. (2011). Long-term evolution of Columbia River tides. *Journal of Waterway, Port, Coastal, and Ocean Engineering*, *137*, 182–191. https://doi.org/10.1061/(ASCE)WW.1943-5460.0000082
Jay, D. A., Leffler, K., Diefenderfer, H. L., & Borde, A. B. (2014). Tidal-fluvial and estuarine processes in the lower Columbia River: I. Along-channel water level variations, Pacific Ocean to Bonneville Dam. *Estuaries and Coasts*, *38*(2), 415–433. https://doi.org/10.1007/s12237-014-9819-0
Devlin, A. T., Jay, D. A., Talke, S. A., & Zaron, E. (2014). Can tidal perturbations associated with sea level variations in western Pacific Ocean be used to understand future effects of tidal evolution? *Ocean Dynamics*, *64*(8), 1093–1120.
Kästner, K., Hoitink, A. J. F., Torfs, P. J. J. F., Deleersnijder, E., & Ningsih, N. S. (2019). Propagation of tides along a river with a sloping bed. *Journal of Fluid Mechanics*, *872*, 39–73. https://doi.org/10.1017/jfm.2019.331
Kennedy, V. S. (1984). *The estuary as a filter*. New York: Academic Press.
Kukulka, T., & Jay, D. A. (2003). Impacts of Columbia River discharge on salmonid habitat: 2. Changes in shallow-water habitat. *Journal of Geophysical Research*, *109*(C3), 3294. https://doi.org/10.1029/2003JC001929
Lamb, M. P., Nittrouer, J. A., Mohrig, D., & Shaw, J. (2012). Backwater and river plume controls on scour upstream of river mouths: Implication for fluvio-deltaic morphodynamics. *Journal of Geophysical Research*, *117*, F01002. https://doi.org/10.1029/2011JF002079
Lanzoni, S., & Seminara, G. (1998). On tide propagation in convergent estuaries. *Journal of Geophysical Research*, *103*(C13), 30,793–30,812. https://doi.org/10.1029/1998JC900015
Le Provost, C. (1991). Generation of overtides and compound tides (review). In B. B. Parker (Ed.), *Tidal hydrodynamics* (pp. 269–295). Toronto: John Wiley.
LeBlond, P. H. (1978). On tidal propagation in shallow rivers. *Journal of Geophysical Research*, *83*, 4717–4721. https://doi.org/10.1029/JC083iC09p04717
LeBlond, P. H. (1979). Forced fortnightly tides in shallow rivers. *Atmosphere Ocean*, *17*(3), 253–264. https://doi.org/10.1080/07055900.1979.9649064
LeBlond, P. H. (1991). Tides and their interactions with other oceanographic phenomena in shallow water (review). In B. B. Parker (Ed.), *Tidal hydrodynamics* (pp. 357–378). Toronto: John Willey.
Lesser, G. R., Roelvink, J. V., Van Kester, J. A. T. M., & Stelling, G. S. (2004). Development and validation of a three-dimensional morphological model. *Coastal Engineering*, *51*, 883–915.
Luo, X. Y., Zhang, W., Chen, S. J., Feng, X., Ji, X. M., & Xu, Y. W. (2020). Evolution of reversal of the lowest low waters in a tidal river network. *Journal of Hydrology*, *585*, 124701. https://doi.org/10.1016/j.jhydrol.2020.124701
MacMahan, J., van de Kreeke, J., Reniers, A., Elgar, S., Raubenheimer, B., Thornton, E., et al. (2014). Fortnightly tides and subtidal motions in a choked inlet. *Estuarine, Coastal and Shelf Science*, *150*, 325–331. https://doi.org/10.1016/j.ecss.2014.03.025
Matte, P., Jay, D. A., & Zaron, E. D. (2013). Adaptation of classical tidal harmonic analysis to nonstationary tides, with application to river tides. *Journal of Atmospheric and Oceanic Technology*, *30*(3), 569–589. https://doi.org/10.1175/JTECH-D-12-00016.1
Matte, P., Secretan, Y., & Morin, J. (2014). Temporal and spatial variability of tidal-fluvial dynamics in the St. Lawrence fluvial estuary: An application of nonstationary tidal harmonic analysis. *Journal of Geophysical Research: Oceans*, *119*, 5724–5744. https://doi.org/10.1002/2014JC009791
Moftakhari, H., Salvadori, G., AghaKouchak, A., Sanders, B., & Matthew, R. (2017). Compounding effects of sea level rise and fluvial flooding. *Proceedings of the National Academy of Sciences*, *114*(37), 9785–9790. https://doi.org/10.1073/pnas.1620325114
Pan, H. D., Lv, X. Q., Wang, Y. Y., Matte, P., Chen, H. B., & Jin, G. Z. (2018). Exploration of tidal-fluvial interaction n the Columbia River Estuary using S_TIDE. *Journal of Geophysical Research: Oceans*, *123*, 6598–6619. https://doi.org/10.1029/2018JC014146
Parker, B. B. (1984). Frictional effects on tidal dynamics of shallow estuary. PhD. Dissertation, The Johns Hopkins University, 291 pp.
Parker, B. B. (1991). The relative importance of the various nonlinear mechanisms in a wide range of tidal interactions. In B. B. Parker (Ed.), *Tidal hydrodynamics* (pp. 237–268). New York: John Wiley.
Pawlowicz, R., Beardsley, B., & Lentz, S. (2002). Classical tidal harmonic analysis including error estimates in MATLAB using T_TIDE. *Computers & Geosciences*, *28*, 929–937. https://doi.org/10.1016/S0098-3004(02)00013-4
Prandle, D. (1991). Tides in estuaries and embayments (review). In B. B. Parker (Ed.), *Tidal hydrodynamics* (pp. 124–148). Toronto: John Wiley.
Pritchard, D. W. (1967). What is an estuary: A physical viewpoint. *American Association for the Advancement of Science*, *83*, 3–5.
Proudman, J. (1953). *Dynamical oceanography* (p. 409). New York: Wiley.
Sassi, M. G., & Hoitink, A. J. F. (2013). River flow controls on tides and tide-mean water level profiles in a tidal freshwater river. *Journal of Geophysical Research: Oceans*, *118*, 4139–4151. https://doi.org/10.1002/jgrc.20297
Savenije, H. H. G. (2005). *Salinity and tides in alluvial estuaries*. Amsterdam: Elsevier Science.
Savenije, H. H. G., Toffolon, M., Haas, J., & Veling, E. J. M. (2008). Analytical description of tidal dynamics in convergent estuaries. *Journal of Geophysical Research*, *113*, 1, C10025. https://doi.org/10.1029/2007JC004408
Song, D. H., Wang, X. H., Kiss, A. E., & Bao, X. W. (2011). The contribution of tidal asymmetry by different combinations of tidal constituents. *Journal of Geophysical Research*, *116*, C12007. https://doi.org/10.1029/2011JC007270
Speer, P. E., & Aubrey, D. G. (1985). A study of non-linear tidal propagation in shallow inlet/estuarine systems. Part II: Theory. *Estuarine, Coastal and Shelf Science*, *21*, 207–224. https://doi.org/10.1016/0272-7714(85)90097-6
Tanaka, H., Hayane, K., Adityawan, M. B., Roh, M., & Farid, M. (2014). Study on the relation of river morphology and tsunami propagation in rivers. *Ocean Dynamics*, *64*, 1319–1332. https://doi.org/10.1007/s10236-014-0749-y
Toffolon, M., & Savenije, H. H. G. (2011). Revisiting linearized one-dimensional tidal propagation. *Journal of Geophysical Research*, *116*, C07007. https://doi.org/10.1029/2010JC006616
Tolkova, E. (2017). Tsunami penetration in tidal rivers, with observations of the Chile 2015 tsunami in rivers in Japan. In *The Chile-2015 (Illapel) earthquake and tsunami* (pp. 315–335). Basel, Switzerland: Springer.
van Rijn, L. C. (2011). Analytical and numerical analysis of tides and salinities in estuaries; part I: Tidal wave propagation in convergent estuaries. *Ocean Dynamics*, *61*, 1719–1741. https://doi.org/10.1007/s10236-011-0453-0
Wang, Z. B., Jeuken, C., Gerritsen, H., de Vriend, H. J., & Kornman, B. A. (2002). Morphology and asymmetry of vertical tide in the Westerschelde estuary. *Continental Shelf Research*, *22*, 2599–2609. https://doi.org/10.1016/S0278-4343(02)00134-6

Wang, Z. B., Juken, H., & de Vriend, H. J. (1999). Tidal asymmetry and residual sediment transport in estuaries. WL|Hydraulic, report No. Z2749, 66 pp.

Zhang, F. Y., Sun, J., Lin, B. L., & Huang, G. X. (2018). Seasonal hydrodynamic interactions between tidal waves and river flows in the Yangtze Estuary. *Journal of Marine Systems*, *186*, 17–28. https://doi.org/10.1016/j.jmarsys.2018.05.005

Zhang, M., Townend, I., Cai, H. Y., & Zhou, Y. X. (2015). Seasonal variation of tidal prism and energy in the Changjiang River estuary: A numerical study. *Chinese Journal of Oceanology and Limnology*, *33*(5), 1–12.

Zhang, M., Townend, I., Zhou, Y. X., & Cai, H. Y. (2016). Seasonal variation of river and tide energy in the Yangtze estuary, China. *Earth Surface Processes and Landforms*, *41*, 98–116. https://doi.org/10.1002/esp.3790

Zhang, W., Cao, Y., Zhu, Y. L., Zhen, J. H., Ji, X. M., Xu, Y. W., et al. (2018). Unravelling the causes of tidal asymmetry in deltas. *Journal of Hydrology*, *564*, 588–604. https://doi.org/10.1016/j.jhydrol.2018.07.023